Thermodynamic and kinetic investigations of the $SrBr_2$ hydration and dehydration reactions for thermochemical energy storage and heat transformation

Jana Stengler [a*], Inga Bürger [a], Marc Linder [a]

[a] Institute of Engineering Thermodynamics, German Aerospace Center (DLR)
Pfaffenwaldring 38-40, 70569 Stuttgart, Germany

*Corresponding author. Tel.: +49 711 6862 8238. E-mail address: jana.stengler@dlr.de

Abstract

The potential of thermochemical energy storage and heat transformation has been soundly highlighted in literature. For applications in the temperature range from approximately 150 °C to 300 °C, the inorganic salt strontium bromide, which reacts with water vapor in an exothermic reaction, is a promising candidate:

$$SrBr_2\ (s) + H_2O\ (g) \rightleftharpoons SrBr_2{\cdot}H_2O\ (s) + \Delta_R H\ .$$

This chemical reaction offers a specific energy density of 291 kJ/kg $SrBr_2$ (or 81 kWh/t). The feasibility of a thermochemical energy storage and heat transformer based on the $SrBr_2/H_2O$ working pair has already been successfully demonstrated on a 1 kW scale in a lab-scale storage unit. Here, we report on the steam pressure-dependent reaction temperatures of the dehydration and hydration reactions as well as the reaction rate and the cycle stability of the reactive system over 100 reaction cycles using thermogravimetric analysis. For distinct operating points, e.g. running the hydration reaction at 180 °C and 69 kPa, specific thermal powers up to 4 kW/kg $SrBr_2$ were experimentally determined. Running the dehydration reaction at 210 °C and 5 kPa steam pressure showed specific thermal powers of 2.5 kW/kg of $SrBr_2{\cdot}H_2O$, thus proving the suitability of $SrBr_2/H_2O$ as thermochemical working pair for high-power storage applications. Our results provide fundamental material-related data for the design of high-power reactor modules as well as for numerical studies on the potential of thermochemical energy storage and heat transformation based on $SrBr_2/H_2O$.

Keywords

Thermochemical energy storage; heat transformation; strontium bromide; thermodynamic equilibrium; thermal hysteresis; gas-solid reaction kinetics

1 Introduction

The potential of thermochemical energy storage and heat transformation to increase the energy efficiency in industrial processes, and thereby to reduce the carbon footprint, is widely discussed in literature [1], [2], [3]. Various types of thermochemical working pairs are investigated for a wide range of operating temperatures, many of them based on gas-solid

reactions. Several material screening studies focus on the criteria which gas-solid reactions need to fulfill in order to be suitable candidates for thermochemical energy storage [4], [5] and heat transformation applications in particular [6], [7]. In short, the most relevant criteria for industrial applications are summarized as follows:

- reversible and cycle-stable reaction in the relevant temperature range,
- sufficient specific energy storage density (kWh/kg),
- high effective reaction rates which allow for large specific thermal powers (kW/kg) ,
- no side reactions, thermal decomposition or melting,
- non-toxic materials and commercial availability.

A promising candidate is the inorganic salt strontium bromide. The dehydration reaction of strontium bromide hexahydrate to the monohydrate was discussed in several studies, e.g. by N'Tsoukpoe et al. [8] for thermal energy storage applications below 105 °C. Michel et al. investigated the monohydrate-hexahydrate reaction in an experimental study with a packed bed reactor operated with 400 kg hydrated salt, and reported thermal powers in the range from 0.75 – 2 W/kg [9]. Besides their experimental studies, the authors developed a two-dimensional model for a rectangular module of the thermochemical storage reactor operated at temperatures below 100 °C [10]. The reaction rates were assumed to depend on the reaction advancement and on the distance from the thermodynamic equilibrium, and a first-order kinetic law was chosen. A more detailed reaction rate model for the hydration reaction from the monohydrate to the hexahydrate form was developed by Esaki et al. for maximum operation temperatures of 80 °C [11]. In another experimental study, a composite material based on strontium bromide hexahydrate and natural graphite was investigated by Cammarata et al. [12]. The authors report an improvement of the hydration reaction progression due to an increased thermal conductivity and a reduced thermal hysteresis. However, no investigation on the cycle stability of the composite material was conducted. Same as in the studies referenced above, this thermochemical system addresses domestic applications with a maximum storage temperature of 100 °C. A possible show stopper in these low-temperature storage applications are the relatively high specific material costs of strontium bromide, since especially seasonal storage applications require high storage capacities. Nevertheless, the production process of strontium bromide on a large industrial scale is not yet optimized and costs may reduce drastically with increasing usage. This issue is addressed by Gilles et al. [13]. The authors investigate an alternative and cost-efficient synthesis pathway to reduce production costs, and also discuss the carbon footprint of strontium bromide when used for low temperature energy storage (< 100 °C).

In contrast, operating a thermochemical reactor with the reacting couple $SrBr_2 \cdot H_2O$ at higher temperatures (> 150 °C) and high specific thermal powers has not been in the spotlight of research yet. This is possible by selecting the thermochemical reaction from the anhydrous phase to the monohydrate,

$$SrBr_2\,(s) + H_2O\,(g) \rightleftharpoons SrBr_2 \cdot H_2O\,(s) + \Delta_R H\,, \qquad \text{Eq. (1)}$$

instead of mono- to hexahydrate. This reaction is listed in a database on salt hydrate pairs by Glasser [14], and thermodynamic data is given with $\Delta_R H^0 = 72.8$ kJ/mol and $\Delta_R S^0 = 152$ J/(mol·K) ($p^0 = 27.4$ Torr, $T^0 = 298$ K). Based on the standard enthalpy and entropy

of formation given in the NBS Tables [15], the reaction enthalpy and entropy are 71.98 kJ/mol and 143.93 J/(mol·K), respectively (p^0 = 0.1 MPa, T^0 = 298 K), which are the values we refer to in the present work. The reaction was identified as a potential candidate for thermochemical heat transformation applications in a previous study by our research group [6]. We found the reaction to be reversible, however, a thermal reaction hysteresis was observed in thermogravimetric analysis (TGA) experiments: at a water vapor partial pressure of 5 kPa, a difference of 22 K between the hydration and dehydration temperatures was found. For 10 dehydration/hydration reactions, cycle-stability was experimentally confirmed. Based on these screening results, we investigated the hydration reaction of strontium bromide on a 1 kg scale [16]. This work led to an experimental proof-of-concept for thermochemical heat transformation with 102 K thermal upgrade and a maximum discharge temperature of 280 °C in a 1 kW lab-scale prototype [17]. During the discharging process, the specific thermal power of the storage module was observed to slightly decrease with increasing discharge temperature and constant steam pressure. In addition, the granular storage material was found to have agglomerated into larger porous structures, thus raising questions on the cycle stability of the chemical reaction.

Therefore, to further clarify the qualification of the $SrBr_2/H_2O$ working pair for industrial energy storage and heat transformation applications in the temperature range from approximately 150 - 300 °C (e.g. waste heat recovery from batch processes in chemical industries), in this work we present a detailed analysis of its cycle stability and thermodynamic and kinetic properties.

2 Experimental methods and data analysis

Two different experimental methods were applied in the presented study: firstly, thermogravimetric analyses with samples on a 15 mg scale, and secondly, investigations with a lab-scale test setup with sample masses of around 1 kg of $SrBr_2 \cdot H_2O$.

2.1 Sample preparation

Strontium bromide was supplied in the form of hexahydrate crystals (strontium bromide hexahydrate, 99%, CAS 7789-53-9, particle size: 0.2 - 1.25 mm, abcr GmbH). The hexahydrate phase melts at a temperature of 89 °C [18], and therefore was dried in a circulating air oven at 70 °C for several hours to obtain the monohydrate form, $SrBr_2 \cdot H_2O$. Full decomposition from the hexahydrate to the monohydrate phase was assured by recording the mass loss. The monohydrate samples were then preserved at 70 - 110 °C until they were investigated with the experimental methods described in the following.

2.2 Thermogravimetric analysis (TGA)

For the kinetic and cycling investigations on milligram scale, two different commercial TGA setups were used: a NETZSCH STA 449C *Jupiter*®, equipped with a water vapor furnace and a steam generator (aDROP by *Bronkhorst)*, and, a NETZSCH STA 449F3 equipped with a humidity generator (MHG32 by ProUmid) and humidity sensor. The two devices mainly differ in the manner of vapor generation and, thereby, in their operation range in respect to the available water vapor partial pressure.

In both devices, a dry flow of nitrogen was used as purge and protective gas. To set the desired vapor partial pressure, the purge gas flow was mixed with water vapor (constant total volumetric flow of 100 ml/min). The volumetric flow of nitrogen used as protective gas stayed at a constant level, and is not considered in the calculation of the water vapor partial pressure (STA 449C: 50 ml/min, STA 449F: 20 ml/min). The TGA devices operate at ambient conditions, and we assumed the ambient pressure to be at a constant value of 97 kPa. In the case of the STA 449C, the resulting water vapor partial pressure was calculated from the set nitrogen volume flow and water mass flow (maximum error ±0.5…1 kPa). In case of the STA 449F, humidity data were obtained from the humidity sensor located right before the gas inlet to the sample chamber. Assuming a humidity sensor measurement accuracy of 2%, and an error in the temperature measurement in the evaporator chamber (Pt100, ±1 K) contributing to the maximum error propagation, this results in a maximum error of 1.3 kPa for typical operation conditions (85 °C evaporator temperature, 5 kPa water vapor partial pressure). A TGA sample mass of 15 ± 1 mg and platinum/rhodium crucibles (STA 449F3, DSC sample carrier with thermocouple Type K, measurement accuracy ±1 K) or alumina crucibles (STA 449C, TG sample carrier with thermocouple Type S, measurement accuracy ±1 K) were chosen. The sampling rate was set to 60 points per minute. To reduce noise, all TGA data were smoothed using the NETZSCH *Proteus*® software (Savitzky-Golay filter, smoothing factors 4 - 6, A).

At the beginning of each TGA experiment, the sample was heated up to 250 °C to obtain the anhydrous phase. The hydration and subsequent dehydration and further reaction cycles were performed under the desired water vapor partial pressure and temperature conditions. From the recorded mass change $\Delta m_{\mathrm{TGA}}(t)$, the reaction conversion $X(t)$ was calculated based on the $SrBr_2 \cdot H_2O$ sample mass, m_{sample}, and molar weights, M:

$$X_{\mathrm{hyd.}}(t) = \frac{\Delta m_{\mathrm{TGA}}(t)}{m_{\mathrm{sample}}} \cdot \frac{M_{\mathrm{SrBr2\cdot H2O}}}{M_{\mathrm{H2O}}} \qquad \text{Eq. (2)}$$

$$X_{\mathrm{dehyd.}}(t) = 1 - \frac{\Delta m_{\mathrm{TGA}}(t)}{m_{\mathrm{sample}}} \cdot \frac{M_{\mathrm{SrBr2\cdot H2O}}}{M_{\mathrm{H2O}}} \qquad \text{Eq. (3)}$$

The reaction conversion is analyzed in isothermal and dynamic (constant heating or cooling rate) experiments in the temperature range from 150 - 210 °C and the water vapor partial pressure range from 0 - 97 kPa. For the later application, this is the operation range relevant for thermally charging the storage at low temperatures, e.g. by using waste heat from industrial processes. For discharging the storage at higher temperatures, higher steam pressures are of interest. However, due to the experimental limitations of the setups, higher pressures could not be investigated in the available TGA devices. For this purpose, a lab-scale test setup was implemented.

2.3 Lab-scale test setup

The lab-scale setup was designed to answer two specific questions: Firstly, the investigation of the general feasibility of the hydration reaction at steam pressures up to approximately 150 kPa, and secondly, detailed investigations on the reaction temperatures of the hydration and dehydration reactions. To investigate the bulk phase of the reactive material, a rectangular packed bed of the reactive material is examined, which is enclosed by single-embossed pillow

plates (see Fig. 1). Via the pillow plates, the reaction chamber is heated by thermal oil, with the most important design consideration being the minimization of heat losses from the $SrBr_2$ packed bed to the ambient. A detailed description of the setup is given in [16]. The test rig that was used to operate the chemical reaction is adapted from former experiments on calcium chloride [19]. The steam pressurizer, which is constructed from a tube bundle heat exchanger with thermal oil on the shell side, serves as condenser during the dehydration, and as evaporator during the hydration process. In the present work, the relevant measurement data recorded during the experiments are the temperature measured at the central position of the bulk phase and the steam pressure in the setup, which is controlled by the set condenser/evaporator temperature (temperature sensor: Pt100 class A, measurement uncertainty ±(0.15 °C + 0.002 ϑ/°C), digitization error ±0.05 K. Pressure sensor: *Endress+Hauser, Cerabar M PMP55*, measurement uncertainty and digitization error ±(0.8 kPa + 0.007 *p*/kPa)).

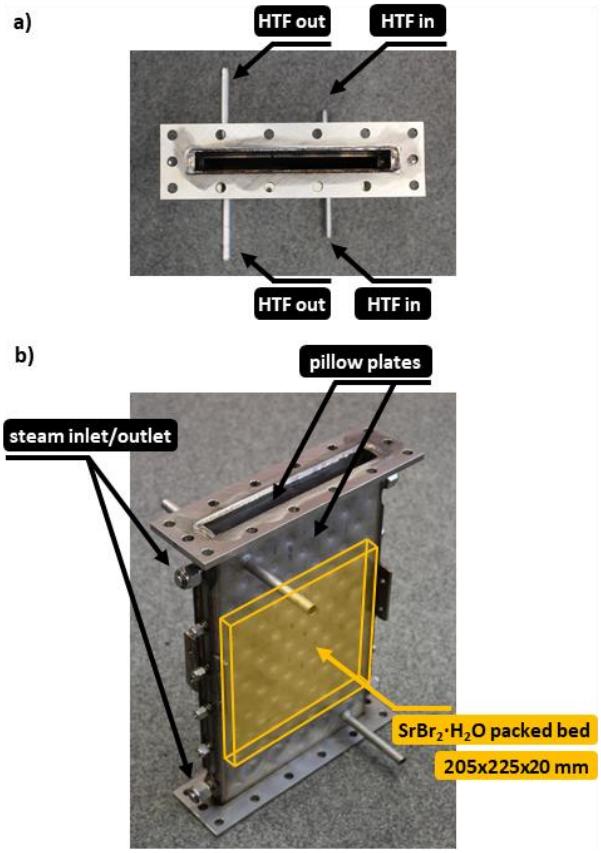

Fig. 1. Pillow plate reaction chamber. a) top view, b) side view. In addition to the aspect of minimized heat losses from the bulk phase to the ambient, the reaction chamber was designed to be easily accessible for temperature sensors. It consists of two single-embossed pillow plates that are mounted with their plane sides back-to-back. This way, a 290 mm x 225 mm x 20 mm space is formed, filled with approximately 1 kg of $SrBr_2{\cdot}H_2O$ (205 mm filling height). The reactive packed bed is fixed by metallic sinter filters with a mesh size of 5 µm. During the dehydration and hydration experiments, the temperature and the flow rate of the heat transfer fluid (HTF) are set to constant values. Pt100 temperature probes are installed in the HTF inlet and outlet, and at several positions within the $SrBr_2{\cdot}H_2O$ fixed bed. In this analysis, the temperature measured at the central position of the fixed bed is evaluated.

The experiments are conducted as follows: before the start of a dehydration experiment, the reactive material is preheated to a constant temperature via the heat transfer fluid. Hence, steam

pressure builds up in the reactive chamber. As soon as the pressure in the reaction chamber drops when connecting the reaction chamber with the condenser, the endothermic reaction starts, indicated by a temperature drop in the solid bulk phase. When the temperature in the fixed bed reaches its initial value, the dehydration reaction is considered to be completed, and the test setup is evacuated to remove all remaining inert gases or steam. Correspondingly, during the hydration process, steam is supplied at a constant evaporation temperature. As soon as the vapor penetrates the solid phase after connecting the reaction chamber with the evaporator, the exothermic reaction starts, thus resulting in a steep rise in the solid temperature. Again, the chemical reaction is assumed to be completed when the bulk phase reaches its initial temperature. For the hydration reaction, we discussed exemplary $T(p,t)$ curves and pressure-dependent maximum reaction temperatures in a prior publication [16]. In this work, we present the corresponding results of the dehydration reaction, i.e. the minimum temperatures which were measured at the central position of the fixed bed for different steam pressures.

2.4 Thermodynamic equilibrium and kinetic modelling of gas-solid reactions

Before we proceed to the discussion of the experimental results, the thermodynamic considerations for the analysis of reversible gas-solid reactions will be discussed in brief.

Assuming ideal gas properties, the equilibrium constant K_{eq} for the gas-solid reaction from Eq. (1) is given by the expression

$$K_{eq}(T,p) = \left(\frac{p}{p^0}\right)^{\nu_{H2O}}, \qquad \text{Eq. (4)}$$

with the stoichiometric coefficient $\nu_{H2O} = 1$ and the reference pressure p^0. In the thermodynamic equilibrium state, the Gibbs free energy is minimized, and Eq. (5) applies:

$$\Delta_R G = \Delta_R G^0 + RT \cdot \ln K_{eq}(T,p) = 0\,. \qquad \text{Eq. (5)}$$

With the definition of the Gibbs free energy of reaction,

$$\Delta_R G^0 = \Delta_R H^0 - T \cdot \Delta_R S^0, \qquad \text{Eq. (6)}$$

we obtain the linear form of the Van't Hoff equation for a reversible gas-solid reaction:

$$\ln K_{eq}(T,p) = \ln\left(\frac{p}{p^0}\right) = -\frac{\Delta_R H^0}{RT} + \frac{\Delta_R S^0}{R}\,. \qquad \text{Eq. (7)}$$

Thus, according to Eq. (7), a $\ln(K_{eq})$ versus $1/T$ graph (Van't Hoff plot) based on the standard molar enthalpy and entropy of the chemical reaction (e.g. calculated from molar enthalpies and entropies of formation) gives an approximation of the equilibrium line. Different methods are established to investigate the thermodynamic equilibrium line of gas-solid reactions, e.g. dynamic TGA measurements with varying gas pressures or long-term pressure measurements in isothermal closed systems. However, in non-ideal thermochemical systems, a thermal hysteresis can arise between the endothermic and the exothermic reactions, e.g. due to kinetic limitations and the occurrence of a metastable zone in the vicinity of the equilibrium line, resulting in two "apparent" equilibrium lines instead of a single one, e.g. such as observed in the case of calcium chloride [20] and copper chloride [21]. This is also the case for the $SrBr_2/H_2O$ reaction system investigated in the present work. In this context, we therefore use the term "pressure-dependent reaction temperature", when we refer to the apparent equilibrium

temperature. Experimental data points on the pressure-dependent reaction temperatures are obtained from the lab-scale setup. These data are evaluated to determine the operation range of the thermochemical working pair.

For the design of high-power storage reactors, not only knowledge on the reaction temperatures is required, but also information on the effective reaction rates, as these might limit the performance of the storage. However, it is important to note that it is not our aim to gain a deep understanding on the actual reaction mechanisms or the physical processes which determine the reaction kinetics of the gas-solid reactions. Instead, we set our focus on establishing application-oriented empirical models for describing the effective reaction rate with regard to the relevant conditions for thermochemical energy storage and heat transformation.
For the parametrization of the empirical reaction rate models, experimental data from TGA measurements are evaluated. Based on the general kinetic equation commonly used for describing the reaction rate in gas-solid reactions, we consider three separate rate-determining terms:

$$\frac{\mathrm{d}X}{\mathrm{d}t} = k(T) \cdot f(X) \cdot h(p) \qquad \text{Eq. (8)}$$

with the temperature-dependent term $k(T)$ according to Arrhenius law, a yield-dependent term $f(X)$, and a vapor pressure-dependent term $h(p)$. For describing the influence of the gas pressure, we chose a term in the form of $h(p) = (1 - p/p^*)^n$, with p* referring to the equilibrium pressure. Hence, for the dehydration reaction, the reaction rate is described as follows:

$$\frac{\mathrm{d}X}{\mathrm{d}t} = A_0 \exp\left\{-\frac{E_a}{\mathrm{R}T}\right\} \cdot f(X) \cdot \left(1 - \frac{p}{p_{\mathrm{dehyd}}}\right)^n, \qquad \text{Eq. (9)}$$

and, correspondingly, for the hydration reaction:

$$\frac{\mathrm{d}X}{\mathrm{d}t} = A_0 \exp\left\{-\frac{E_a}{\mathrm{R}T}\right\} \cdot f(X) \cdot \left(\frac{p}{p_{\mathrm{hyd}}} - 1\right)^n. \qquad \text{Eq. (10)}$$

The kinetic parameters (pre-exponential factor A_0, activation energy E_a, conversion-depending reaction model function $f(X)$, and pressure term exponent n) are fitted from isothermal and isobaric TGA experiments. The detailed fitting procedure is described in section 3.3.

3 Results and discussion

Using the experimental methods and data analysis procedures described above, the thermochemical working pair $SrBr_2/H_2O$ is investigated with regard to its operation range for energy storage and heat transformation. Data on the dehydration reaction temperature and kinetics are necessary to better understand the limiting processes during the charging phase of the storage, which we assume to take place at temperatures as low as possible in industrial applications. In contrast, the hydration reaction determines the maximum discharge temperature and thermal power of the storage, given that steam is supplied as gaseous reactant at a certain maximum pressure, e.g. determined by the maximum available waste heat temperature. And, lastly, cycle stability of the chemical reaction is a basic prerequisite in all kinds of industrial storage and heat transformation applications.

3.1 Investigations on the dehydration and hydration reaction temperatures

As described above, data on the thermodynamic equilibrium of gas-solid reactions are commonly determined from dynamic (non-isothermal) TGA measurements. Usually, sets of dynamic experiments with varying vapor pressures are performed, and the onset temperatures are evaluated [22]. As the onset temperature also depends on the heating rate (dehydration) or cooling rate (hydration), respectively, measurements are conducted at different rates. The onset temperatures are extrapolated to a rate of 0 K/min, which gives the estimated equilibrium temperature for a corresponding vapor partial pressure.

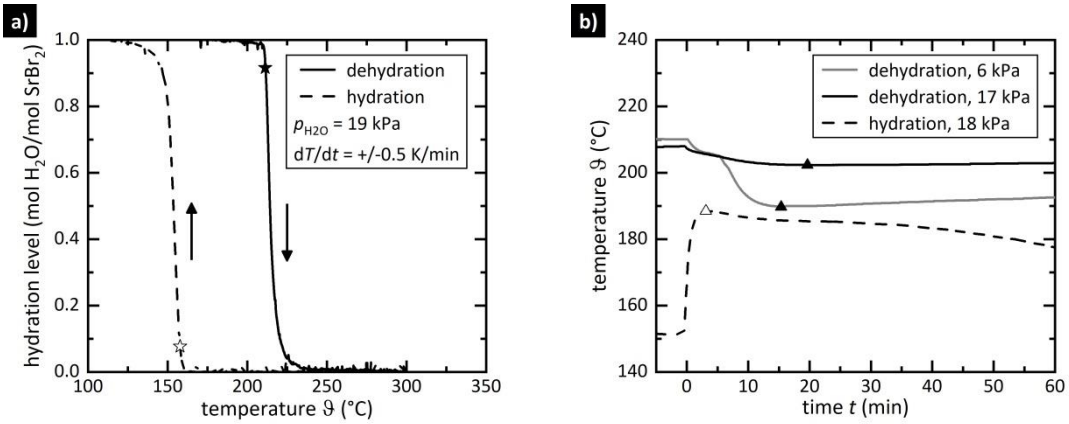

Fig. 2. a) Investigation of the dynamic dehydration and hydration reaction with thermogravimetric analysis (TGA). Resulting level of hydration for p = 19 kPa and a heating/cooling rate of +/-0.5 K/min. A hysteresis of 53 K is found between the hydration and dehydration onset temperatures (☆, ★). b) Investigation of the pressure-dependent reaction temperatures in the lab-scale setup. For a similar steam pressure as in the TGA experiments (hydration: 18 kPa, dehydration: 17 kPa), a significantly smaller hysteresis of 14 K between the reaction temperatures (△,▲) is observed. When the pressure was lowered to 6 kPa in the dehydration process, a reaction temperature of 189 °C was reached. In comparison to the 188 °C hydration data point, this corresponds to a hysteresis of approximately 12 kPa in terms of the pressure offset between the back and forward reaction at the same temperature.

However, following this procedure for the reaction system $SrBr_2/H_2O$, a kinetic limitation was found which led to unexpectedly low hydration temperatures. For example, for heating/cooling rates of ±0.5 K/min and a water vapor partial pressure of 19 kPa, the onset temperature of the dehydration reaction was 211 °C, whereas for the hydration reaction at the same vapor pressure, an onset temperature of 158 °C was found, thus resulting in a thermal hysteresis of 53 K (see Fig. 2a).

In contrast to these dynamic TGA experiments, where a specific temperature profile is applied on the $SrBr_2$ sample, the experiments with the lab-scale setup are conducted at constant preheat temperatures. However, no significant heat flux is introduced into or withdrawn from the reactive material during the reaction. Hence, a characteristic temperature plateau builds up in the bulk phase. These characteristic plateaus correspond to a minimum temperature in the case of the endothermic dehydration reaction, and to a maximum temperature in the case of the exothermic hydration reaction.

Compared to the TGA experiments at similar vapor (partial) pressures, our results from the lab-scale experiment show slightly lower dehydration temperatures (202 °C reaction temperature vs. 211 °C onset temperature) and significantly higher hydration temperatures (188 °C reaction temperature vs. 158 °C onset temperature). Thus, in the lab-scale experiment, the thermal hysteresis is reduced to 14 K between the dehydration of the monohydrate and the hydration of the anhydrous phase (see Fig. 2b). This finding indicates that the onset temperatures determined from dynamic TGA experiments are dominated by a kinetic limitation, and therefore do not lead to a reliable evaluation of the thermodynamic equilibrium state. Obviously, the lab-scale setup results are much closer to the actual thermodynamic equilibrium. As described by Sögütoglu et al., a metastable zone in the vicinity of the of the equilibrium line can be described by nucleation and growth processes [21]. Based on their findings, the kinetic limitation observed in the TGA experiments on the $SrBr_2$ hydration reaction could be explained by the formation of nuclei, with the nucleation rate limiting the overall conversion in the metastable zone. This could lead to the lower hydration onset temperature found in the dynamic TGA experiment. In contrast, in the lab-scale setup with a sample mass of around 1 kg, the existence of nucleation sites already at the very beginning of the hydration reaction is very likely, e.g. due to a remainder of some only partially dehydrated crystals in the packed bed. These already available nucleation sites could instantaneously trigger the hydration reaction, thus leading to higher apparent equilibrium temperatures in the lab-scale setup. Hence, to obtain the pressure-dependent reaction temperatures of the hydration and the dehydration reactions, we use the lab-scale setup which features reaction conditions more representative for potential storage applications.

One key finding of those lab-scale experiments is that the temperature plateaus are solely determined by the steam pressure, and do not depend on the preheat temperature of the bulk phase, which is set via the heat transfer fluid temperature. Corresponding exemplary experiments with a variation of the steam pressures and preheat temperatures are presented in Fig. 3. Based on these results, we conclude that from the temperature plateaus, the pressure-dependent reaction temperatures of the chemical reaction can be derived in sufficient approximation.

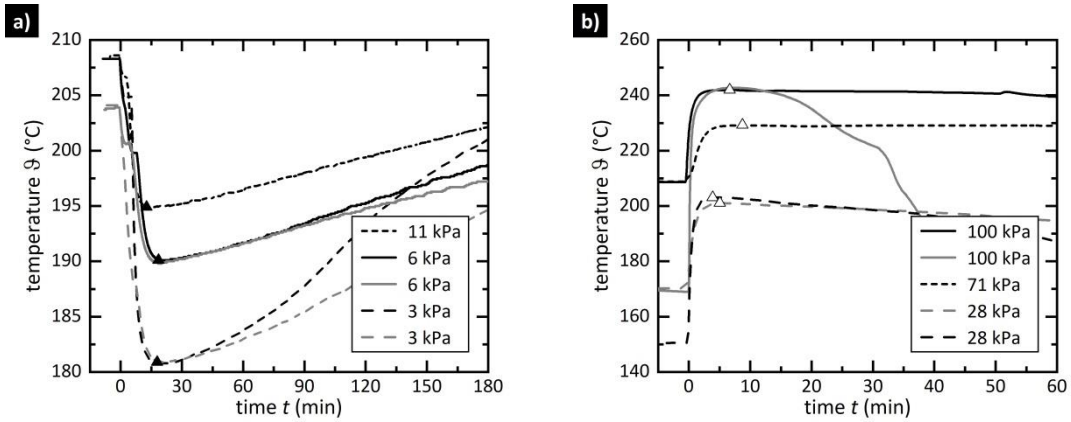

Fig. 3. Investigation of the reaction temperatures in the lab-scale setup for different steam pressures and preheat temperatures. The differing preheat temperatures can be read from the isothermal conditions before the start of the experiment (t = 0 min). The resulting plateau temperatures (△,▲) are evaluated as a function of the corresponding pressure data. a) Dehydration reaction. b) Hydration reaction.

The resulting temperature-pressure data pairs are plotted in the Van't Hoff graph in Fig. 4 for a total of 75 experiments, conducted with three different batches of $SrBr_2 \cdot H_2O$. In this experimental series, the steam pressures as well as the preheat temperatures were varied. The experimental results reveal that there still is a thermal hysteresis between the endothermic and the exothermic reaction, but that it is significantly smaller than found in dynamic TGA experiments. We assume this hysteresis to be caused by a similar mechanism as discussed for the TGA experiments, which is presumably more significant at lower temperatures. For experimental reasons (the maximum thermal oil temperature is limited to 210 °C), higher dehydration pressures could not be investigated in the available setup. Additional experiments would hence be needed to fully clarify if the two lines merge into one at higher steam pressures (and thus, at higher absolute temperatures), as it is the case e.g. for the hydration reaction of CaO and dehydration of $Ca(OH)_2$, respectively [23].
In order to account for the drifting apart of the reaction temperatures from the equilibrium line for pressures below approximately 30 kPa, the dehydration and the hydration data points were fitted by linear regression:

dehydration reaction: $$\log(p_{\mathrm{dehyd}}/\mathrm{kPa}) = 14.69 - 6.41 \cdot \frac{10^3}{T/\mathrm{K}} \qquad \text{Eq. (11)}$$

hydration reaction: $$\log(p_{\mathrm{hyd}}/\mathrm{kPa}) = 8.18 - 3.19 \cdot \frac{10^3}{T/\mathrm{K}} \qquad \text{Eq. (12)}$$

These correlations of the steam pressure and the reaction temperatures give a first estimation of the operation range of a thermochemical storage and heat transformer operated with the $SrBr_2/H_2O$ working pair. E.g., we conclude that a minimum temperature of 170 °C will be required to charge the storage, even if the steam pressure is kept below 2 kPa (15 °C condensation temperature), which can be considered a lower limit in industrial applications due to the needed cooling effort. The two p,T-correlations from Eq. (11) and Eq. (12) are used in the analysis on the effective hydration and dehydration reaction rates later on.

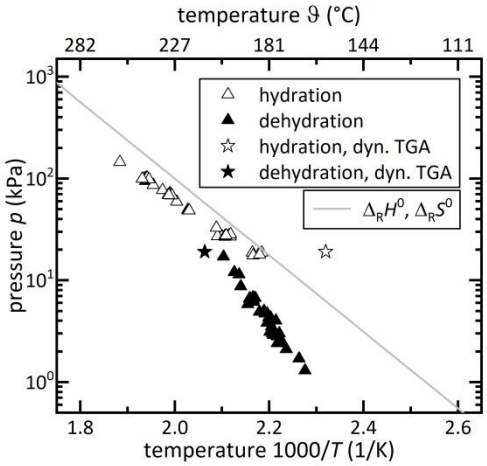

Fig. 4. Van't Hoff plot of the experimental results on the dehydration and hydration reaction temperatures. In addition to the pressure-dependent, characteristic temperature plateaus found in experiments with the lab-scale setup (△,▲), the plot contains data from dynamic TGA measurements (☆,★). These two experiments were conducted at a heating and cooling rate of +/-0.5 K/min and, despite this low rate, reveal a thermal hysteresis which is significantly larger than the one observed in the lab-scale experiments. The thermodynamic data $\Delta_R H^0$ = 72.8 kJ/mol and $\Delta_R S^0$ = 152 J/(mol·K) are given for the reference pressure p^0 = 0.1 MPa, and temperature T^0 = 298 K [15].

3.2 Cycle stability

After having identified the operation range of the reversible chemical reaction, probing the cycle stability is the next crucial hurdle to qualify the $SrBr_2/H_2O$ working pair for any industrial storage application. As 170 °C is identified as the minimum required charging temperature, this value is chosen as reference temperature for isothermal cycling TGA experiments. In this analysis, the progression of the reaction conversion is evaluated.

100 hydration/dehydration cycles were performed at the constant temperature of 170 °C (STA 449 F3 with humidity sensor): In the hydration phase, the water vapor partial pressure was set to 30 kPa (relative humidity of 51% at 85 °C) for the duration of one hour. This humidity condition was chosen as it allows for full conversion to the monohydrate within less than 10 minutes. Subsequently, the relative humidity in the sample chamber was set to 0% for one hour, except for the last dehydration phase (cycle #100), which was set to three hours under dry atmosphere. The humidity was measured in the gas mixing chamber next to the inlet of the sample chamber. When analyzing the recorded humidity for the given TGA operation conditions, we observed that it takes less than 2 minutes to reach 80% of the set humidity during the hydration phase, but approximately 10 minutes until a dry atmosphere is obtained in the sample chamber in the dehydration phase. This temporal offset, which depends on the TGA parameters (e.g. prior and set humidity, gas volume flow and temperatures) causes a dead time until the reaction in the TGA sample chamber starts, both in the case of the dehydration and the hydration reaction.

In the analysis on the reaction conversion calculated from the mass loss or gain during cycling, it is assumed that at the end of a hydration phase, i.e. after 60 min under humid atmosphere, a full reaction conversion of $X_{hyd} = 1$ is reached. The progression of the reaction conversion from cycle #1 up to cycle #100 is displayed in Fig. 5. It is found that the phase transition from the monohydrate to the anhydrous phase and reverse is cycle stable, although the rate of the dehydration reaction deccelerates considerably during the cycling series especially for the "tail" of the reaction progression.

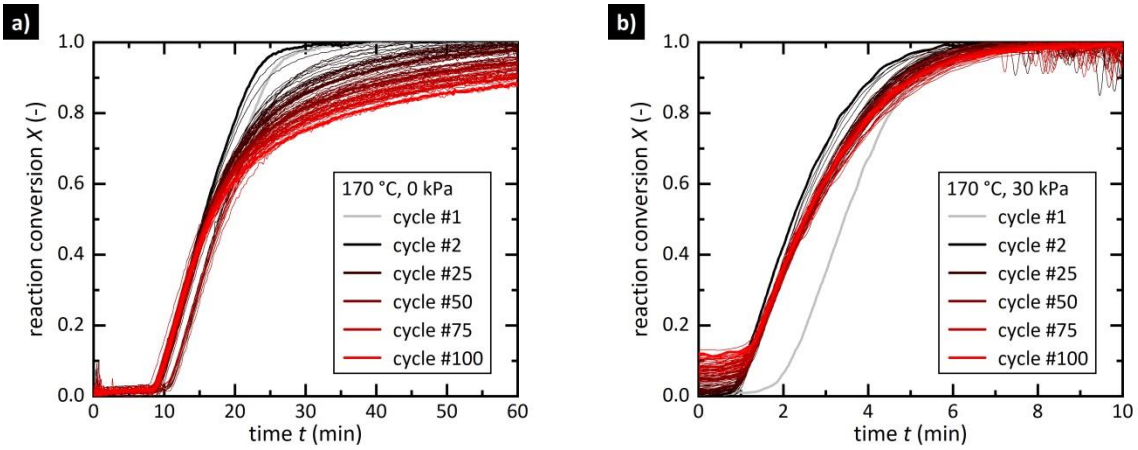

Fig. 5. Cycle stability in terms of the reaction progression during isothermal cycling. Data from different cycles are indicated by changing colors from black to red, with examples shown in the legend for orientation. a) Isothermal dehydration at 170 °C sample temperature and dry nitrogen atmosphere. b) Isothermal hydration at 170 °C sample temperature and a water vapor partial pressure of 30 kPa.

While in the 1st dehydration cycle, full conversion is already reached within approximately 20 minutes, the 100th dehydration is completed only after three hours (not shown in the graph). Although the hydration reaction was observed to slightly deccelerate too, the effect is less significant. The first hydration reaction apparently has an offset compared to all the later cycles, even though the qualitative trend is very similar to the next cycles. We assume this to be caused by the experimental conditions in the setup, e.g. humidification of the sample chamber walls and piping, as the equipment was purged with nitrogen for several hours before the start of the experiment. Similarly, we consider the larger dead times in several of the dehydration cycles to be experimental artefacts caused by deviant humidity conditions in the setup.

As the experimental cycle time was fixed to one hour each for the hydration and the dehydration runs, the decomposition reaction did not reach full yield after several cycles, and therefore the hydration reaction did not start from the hydration level 0.0 mol H_2O/mol $SrBr_2$ for higher cycle numbers. The impact of the rate-decelarating effect is quantifiable from the analysis presented in Fig. 6, which gives the experimental time until 50% and 80% of the expected full conversion are reached. The time constants do not change for the hydration and, in the case of 50% conversion, also for the dehydration reaction. In contrast, the 80% time constant in case of the dehydration rises linearly. Over the course of 100 hydration/dehydration cycles, this time constant increases by approximately 60%. We assume this to be caused by microscopic changes within the $SrBr_2 \cdot H_2O$ phase, e.g. causing inhibited vapor mass transfer, or by some effect on

the reaction kinetics of the dehydration reaction. It is not clear from this experiment, if and when any steady state is reached.

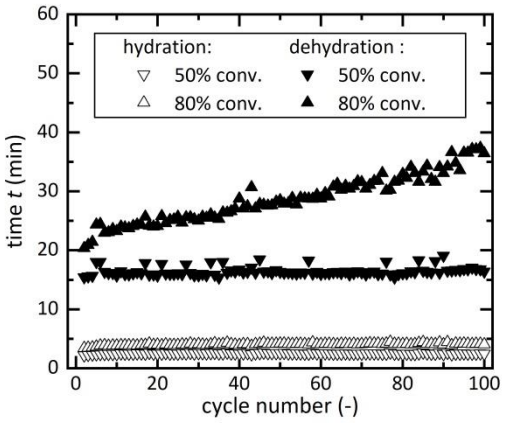

Fig. 6. Evaluation of the cycle stability in terms of the experimental time required to reach 50% and 80% reaction conversion. While the hydration reaction can be considered to be fully cycle-stable under the given experimental conditions (170 °C, 30 kPa water vapor partial pressure), a decrease of the effective reaction rate of the dehydration reaction is found at reaction conversions larger than 50% (170 °C, dry nitrogen atmosphere).

Please note that this cycling series was performed under "extreme" experimental conditions, i.e. the minimum temperature required to perform the dehydration reaction on a reasonable time scale (< 1 hour in TGA experiments). We believe this very low temperature of 170 °C to be hardly realistic for charging the storage in an industrial application as this requires very low steam pressures (< 2 kPa or 15 °C condensation temperature). Therefore, in order to understand how the cycling affects the dehydration behaviour at higher temperatures and pressures which are likely to be more relevant in industrial applications, additional experiments were performed with the cycled $SrBr_2$ sample and compared to an uncycled sample in an identical experiment. At the beginning of these experiments, the samples were treated with the usual heating procedure up to 250 °C to ensure complete dehydration to the anhydrous phase. Fig. 7 contrasts the results obtained for the cycled $SrBr_2$ with the results from the uncycled $SrBr_2$. In all cases, the reaction conversion exceeds 95%, with no significant differences between cycled and uncycled samples (< 3%) with the given measurement accuracy. For better comparison of the reaction progression, the conversion is normalized to a value of 1 in Fig. 7. As the dead time varies due to the different experimental conditions, the curves are shifted along the time axis. The onset time t = 0 min is determined by the intercept point of a tangent fitted at X_{norm} = 0.1 with the time axis. It is observed that at higher dehydration temperatures (210 °C), the reaction conversion of the cycled material is very similar to the behavior of uncycled material: the progression of the dehydration reaction at 210 °C and a dry nitrogen atmosphere, and also under a water vapor partial pressure of 10 kPa, is not affected in any way similar to the dehydration behavior under the cycling series conditions (170 °C, 0 kPa). This is a very important finding since it proves that the lacking cycle stability indicated by Fig. 6 is only of little relevance under application-relevant operation temperatures. Also, this observation supports the assumption that cycling may affect the reaction kinetics of the dehydration reaction, but not the "chemical" reversibility of the dehydration reaction.

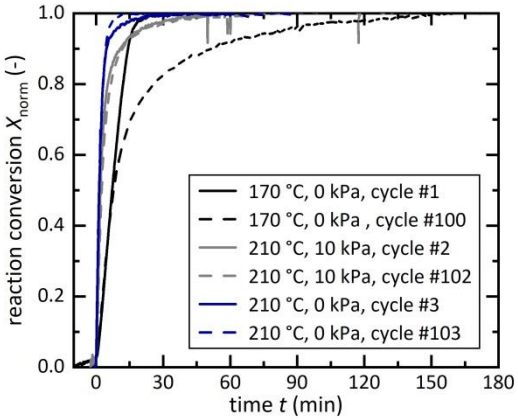

Fig. 7. Progression of the dehydration reaction conversion of cycled and uncycled $SrBr_2 \cdot H_2O$. For better comparison, the conversion is normalized and the reaction onset time is set to 0 in this graph. These experiments prove the cycle stability of the $SrBr_2/H_2O$ working pair over 100 hydration/dehydration cycles.

No macroscopic changes were visible to the bare eye when the $SrBr_2$ sample was optically investigated after the completion of the experimental series. The granules did not agglomerate, but were still loose and easily pourable. However, this does not give information on cycling-induced microscopic transformations within the $SrBr_2$ particles.

Summing up, from the experimental study on the cycle stability of the monohydrate formation and decomposition, we conclude that the reaction is chemically reversible, although the reaction rate of the dehydration reaction decreases in the course of the cycling at low temperatures (170 °C). Given that this degradation effect is not observed when the cycled material is investigated at higher temperatures (210 °C), and moreover, that the degradation could likely be eliminated by pretreating the $SrBr_2 \cdot H_2O$ particles (e.g. milling to obtain smaller primary particles) or using rate-accelerating additives, our results indicate that the reaction system $SrBr_2/H_2O$ is indeed a promising candidate for thermochemical energy storage and heat transformation, with applications requiring large numbers of charging/discharging cycles. Besides, the progression of the dehydration reaction conversion performed under application-relevant operation conditions (210 °C and 10 kPa, corresponding to 45 °C condensation temperature) shows that 80% of the full conversion is reached after approximately 5 minutes, thus highlighting that the $SrBr_2/H_2O$ working pair promises high specific thermal powers due to fast reaction kinetics. This last point is discussed in more detail in the following section.

3.3 Empirical models of the effective reaction rates

Not only the thermodynamic properties (i.e. pressure-dependent reaction temperatures), but also the reaction kinetics determine a thermochemical storage's operation range since the maximum thermal power of the thermochemical reactor is limited by the effective rate of the chemical reaction. To be able to assess the maximum thermal powers allowed by the effective rate of reaction, kinetic data on the reaction progression are required, which include the temperature and pressure range relevant for typical storage applications. However, due to the operational limitations of the TGA setups, this range is restricted to operation under atmospheric pressures and adjusting the steam pressure by dilution with nitrogen. In the following analysis, it is therefore assumed that running the chemical reaction at water vapor partial pressures instead of pure steam atmosphere does not affect the reaction progression. This is considered a valid assumption due to the milligram sample size, so that the formation of a nitrogen boundary layer (which could limit vapor transport) can be neglected. Please note that the aim of this section is not to understand the reaction mechanism in depth, but rather to provide the simplest empirical model with sufficient resolution for the investigation of potential applications.

Based on the qualitative progression of the reaction conversion presented in the investigation on the cycle stability, a single-step reaction progression is assumed. Besides, the trends of the reaction conversion of uncycled material suggest that a bounded exponential growth model is appropriate to mathematically describe the effective reaction rates. Hence, we chose the first-order rate model for both the dehydration reaction and the hydration reaction [24] :

$$X(t) = 1 - \exp(-k_{\mathrm{eff}} \cdot t), \qquad \text{Eq. (13)}$$

With the thereby given linear correlation between –ln(1-*X*) and *t*, effective rate coefficients $k_{\mathrm{eff,exp}}$ were determined by fitting results from TGA experiments similar to the cycling experiments from Fig. 5 conducted under isothermal and isobaric conditions. The rate curves *X*(*t*) are normalized to 1. In the non-normalized data, the average reaction conversion is 1.00, with a standard deviation of 2%. The minimum and maximum values range from 0.95 to 1.05. We assume that the reaction yielded full conversion in the experiments evaluated in context of the reaction rate determination, and attribute the error to measurement inaccuracies, e.g. due to partial hydration during weighing of the monohydrate samples under ambient conditions. The results of the evaluation on $k_{\mathrm{eff,exp}}$ are summarized in Tab. 1 (dehydration reaction) and Tab. 2 (hydration reaction).

Considering the rate of reaction derived from Eq. (13),

$$\frac{\mathrm{d}X}{\mathrm{d}t} = k_{\mathrm{eff}} \cdot (1 - X) = k_{\mathrm{eff}} \cdot f(X), \qquad \text{Eq. (14)}$$

and the rate model proposed in Eq. (8), it follows that k_{eff} gives all the necessary information on the activation energy E_a, the pre-exponential factor A_0, and the exponent *n* of the pressure term:

dehydration reaction: $$k_{\mathrm{eff}} = A_0 \exp\left\{-\frac{E_a}{\mathrm{R}T}\right\} \cdot \left(1 - \frac{p}{p_{\mathrm{dehyd}}}\right)^n \qquad \text{Eq. (15)}$$

hydration reaction: $$k_{\mathrm{eff}} = A_0 \exp\left\{-\frac{E_a}{\mathrm{R}T}\right\} \cdot \left(\frac{p}{p_{\mathrm{hyd}}} - 1\right)^n . \qquad \text{Eq. (16)}$$

The further reaction rate analysis is discussed separately for the hydration and dehydration reactions in the following sections.

Tab. 1. Effective rate coefficients $k_{\mathrm{eff,exp}}$ of the dehydration reaction under isothermal and isobaric conditions. ΔT gives the difference between the experimental temperature T and the reaction temperature T_{dehyd} expected for the given water vapor partial pressure p. R^2 gives the coefficients of determination of the linear fit of the experimental data, which is evaluated in the range from X_{min} to X_{max}.

T (°C)	p (kPa)	T_{dehyd} (°C)	ΔT (K)	$k_{\mathrm{eff,exp}}$ (10^{-3}/s)	R^2 (-)	X_{min} (-)	X_{max} (-)
162	0	--	--	1.08	0.921	0.05	0.80
172	0	--	--	1.82	0.938	0.05	0.80
185	0	--	--	3.20	0.974	0.05	0.80
190	0	--	--	4.20	0.987	0.05	0.80
210	0	--	--	8.69	0.997	0.05	0.80
210	0	--	--	9.01	1.000	0.05	0.80
185	5	185	≈ 1	1.47	0.987	0.10	0.60
190	5	185	5	3.25	0.987	0.05	0.80
200	5	185	15	5.26	0.996	0.05	0.80
210	5	185	25	9.21	0.998	0.05	0.80

Tab. 2. Effective rate coefficients $k_{\mathrm{eff,exp}}$ of the hydration reaction under isothermal and isobaric conditions. ΔT gives the difference between the experimental temperature T and the reaction temperature T_{hyd} expected for the given water vapor partial pressure p. R^2 gives the coefficients of determination of the linear fit of the experimental data, which is evaluated in the range from X_{min} to X_{max}.

T (°C)	p (kPa)	T_{hyd} (°C)	ΔT (K)	$k_{\mathrm{eff,exp}}$ (10^{-3}/s)	R^2 (-)	X_{min} (-)	X_{max} (-)
186	69	230	-44	12.98	0.996	0.06	0.95
192	69	230	-38	8.19	0.985	0.05	0.90
200	69	230	-30	3.84	0.992	0.05	0.85
203	69	230	-27	2.35	0.996	0.05	0.85
207	69	230	-23	1.38	0.994	0.05	0.65
180	29	202	-22	1.54	0.997	0.05	0.85
180	36	209	-28	3.46	0.984	0.05	0.90
180	45	216	-36	8.06	0.991	0.05	0.80
180	55	223	-42	13.20	0.986	0.05	0.95
151	45	216	-65	65.63	0.964	0.05	0.95

3.3.1 Parametrization of the dehydration reaction rate model

The dehydration reaction of the monohydrous salt was investigated in isothermal experiments performed at low water vapor partial pressures (STA 449F3 with humidifier and humidity sensor). To account for the temperature-dependency of the dehydration reaction rate, the first parameter being assessed from an Arrhenius plot is the activation energy E_a. and the pre-exponential factor A_0, see Fig. 8a. In this analysis, data from TGA experiments in dry nitrogen atmosphere are evaluated, since this way the vapor pressure influence on the reaction rate can be neglected. The temperatures in the considered experiments vary in the range from 160 °C to 210 °C, and the analysis gives the two parameters E_a = 75.7 kJ/mol and $A_0 = 1.38 \cdot 10^6$ 1/s.

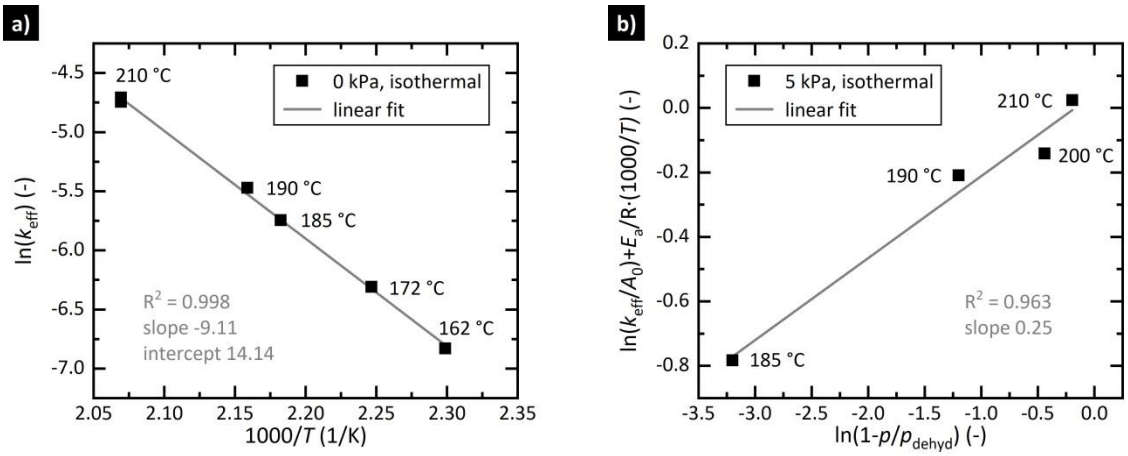

Fig. 8. Dehydration reaction. a) Determination of the activation energy E_a from the slope and the pre-exponential factor A_0 from the offset of the linear regression (Arrhenius plot). Only experiments conducted under dry nitrogen atmosphere are evaluated in this analysis. b) Determination of the pressure term exponent. Here, experiments conducted under 5 kPa water vapor partial pressure and different temperatures are evaluated.

In the next step, the pressure term exponent n is fitted from dehydration experiments in humid atmosphere. In this analysis, experiments at a constant water vapor partial pressure of 5 kPa and different temperatures were considered, as these values are relevant for industrial applications and, besides, correspond to the operation conditions investigated in the proof-of-concept of the $SrBr_2/H_2O$ working pair in a 1 kW storage module [17]. From the plot given in Fig. 8b, we obtain the parameter n = 0.25.

Hence, the empirical rate model of the dehydration reaction is parametrized as follows:

$$\frac{\mathrm{d}X}{\mathrm{d}t} = 1.38 \cdot 10^6 \mathrm{s}^{-1} \exp\left\{-\frac{75.7\ \mathrm{kJ \cdot mol^{-1}}}{\mathrm{R}T}\right\} \cdot (1 - X) \cdot \left(1 - \frac{p}{p_{\mathrm{dehyd}}}\right)^{0.25} . \quad \text{Eq. (17)}$$

The reaction pressure p_{dehyd} for the given temperature is derived from the experimental results of the lab-scale setup, and can be obtained from Eq. (11).

3.3.2 Parametrization of the hydration reaction rate model

The hydration reaction was investigated in isothermal experiments performed at higher water vapor partial pressures (STA 449C with steam generator). Following the same procedure as in the case of the dehydration reaction, the effective rate coefficients $k_{\mathrm{eff,exp}}$ are calculated based on a first-order rate model, see Tab. 2. Notably, the results indicate that at constant vapor pressures and varying temperatures, the rate coefficients actually decrease with increasing temperature (or decreasing temperature difference ΔT).

This is explained by the pressure term in Eq. (10) (last term): an increased temperature leads to a higher reaction pressure p_{hyd}, thus resulting in a smaller ratio p/p_{hyd}, which lowers the overall reaction rate. In the considered temperature and pressure range, this rate-limiting effect of the pressure term overbalances the rate-increasing impact of the Arrhenius term. If these k_{eff} data were fitted in an Arrhenius plot (compare Fig. 8a for the dehydration reaction), this would result in a physically nonsensical negative activation energy. This is not an uncommon phenomenon for gas-solid reactions showing a rate decrease in the vicinity of the equilibrium line. For instance, a virtual negative activation energy was also observed for the hydration reaction of calcium oxide [25]. A non-parametric modelling method such as proposed by Birkelbach et al. is one approach to address such kind of a reaction rate behavior [26]. However, since in this work we pursue an application-oriented empirical correlation on the hydration reaction rate, we set aside the determination of the Arrhenius parameters (pre-exponential factor A_0, activation energy E_a) from the experimental data. Instead, based on the assumption of a first-order rate model, we simplify Eq. (16) by replacing the Arrhenius term by a constant, and obtain the following equation:

$$k_{\mathrm{eff}} = K_{\mathrm{Fit}} \cdot \left(\frac{p}{p_{\mathrm{hyd}}} - 1 \right)^{n}. \qquad \text{Eq. (18)}$$

Provided that this mathematical approach is valid, plotting the data points $\ln(k_{\mathrm{eff}})$ versus $\ln(p/p_{\mathrm{hyd}}\text{-}1)$ should result in a straight line, with the slope n and the offset $\ln(K_{\mathrm{Fit}})$. Indeed, the experimental data displayed in Fig. 9a indicate that this simplification of the rate model is justified. The slope of the linear fit gives the pressure term exponent $n = 1.8$. The rate coefficient $K_{\mathrm{Fit}} = 1.60 \cdot 10^{-3}$ 1/s is determined from the intercept.

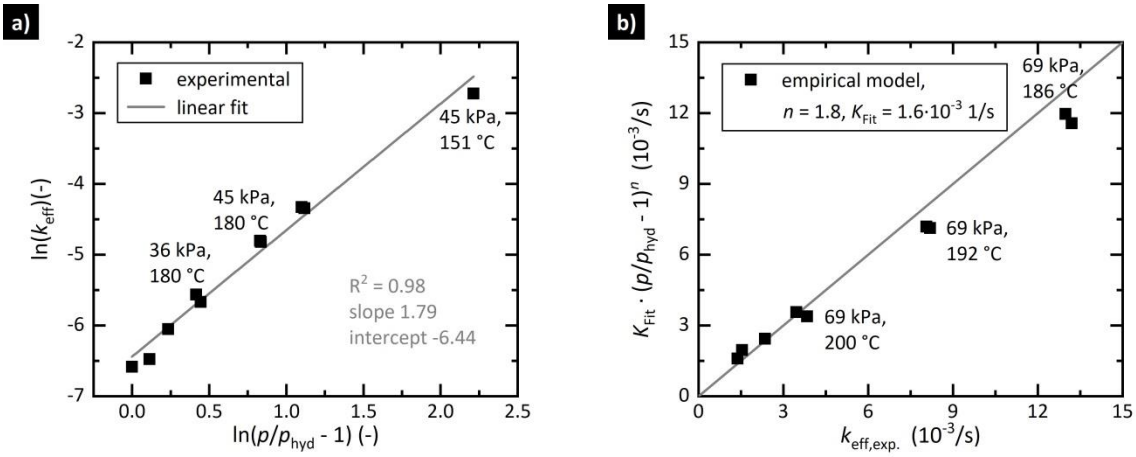

Fig. 9. Parametrization of the hydration rate model. a) The pressure term exponent n is determined from the slope, and the rate coefficient K_{Fit} from the intercept of the linear fit. b) Validity evaluation of the effective rate coefficients predicted by the empirical model, which is parametrized with the values n and K_{Fit} determined from the left plot. The bisectrix in the parity plot indicates an ideal reproduction of the experimental rate coefficients.

Therefore, the parametrized rate model of the hydration reaction results in:

$$\frac{\mathrm{d}X}{\mathrm{d}t} = 1.60 \cdot 10^{-3}\ \mathrm{s}^{-1} \cdot (1 - X) \cdot \left(\frac{p}{p_{\mathrm{hyd}}} - 1\right)^{1.8}. \qquad \text{Eq. (19)}$$

The reaction pressure p_{hyd} for the given temperature is derived from the experimental results of the lab-scale setup, and can be obtained from Eq. (12). Due to the simplification of the hydration rate model, i.e. due to omitting the rate-diminishing Arrhenius term, the model will at some point fail to correctly reproduce the decrease of the rate with decreasing temperatures. Instead, the model given in Eq. (19) would predict infinitely increasing reaction rates with decreasing temperatures. Hence, predicting a "cold start" of the hydration reaction from initial temperatures of more than approximately 65 K below the expected reaction temperature (compare maximum values of ΔT given in Tab. 2) could lead to incorrect results. Apart from that, in the particular case of the $SrBr_2/H_2O$ reaction system, starting from "too low" temperatures (e.g. ambient temperature) would lead to a hydration reaction not only from the anhydrous salt to the monohydrate, but also from the monohydrate salt to the hexahydrate, and then to an unwanted solid-liquid phase change at higher temperatures.

Although Eq. (19) is based on a simplified rate model approach, the effective rate coefficients are reproduced with good accuracy. This is indicated by the evaluation presented in the form of a parity plot in Fig. 9b, which contrasts the predicted with the experimental rate coefficients. The rate-diminishing effect of increased temperatures is correctly reproduced. However, for operation parameters resulting in larger rates, e.g. 69 kPa and 186 °C, the model slightly underrates the experimental values.

3.3.3 Model evaluation

In a last step, the empirical models are evaluated by comparison with the experimentally determined reaction conversions from the TGA experiments. Fig. 10 shows the modelled reaction conversions (line plots) versus the experimental results (scattered plots) for varying operation conditions. For all of the depicted graphs, the results from the empirical models are

shifted along the time axis so that the point $X_{norm} = 0.5$ corresponds to the same point of the experimental curve in order to compensate for the dead time caused by the TGA experimental conditions.

Generally, the qualitative trends of the reaction conversions are correctly reproduced by the empirical models. In the case of the dehydration, the rate-increasing impact of the temperature is clearly indicated by the model (e.g. 5 kPa, 190 °C versus 210 °C). For higher rates, e.g. 10 kPa and 210 °C, the slope of the reaction conversion is closely reproduced by the empirical model up to a conversion of 80%, even though the parametrization of the rate model was implemented based on a data set with a maximum dehydration vapor pressure of 5 kPa. For low dehydration rates, e.g. 170 °C and dry nitrogen atmosphere, the model underrates the dehydration progression of $SrBr_2 \cdot H_2O$. Here, the reaction conversion follows a more sigmoidal trend and, hence, is not closely represented by a first-order rate model.

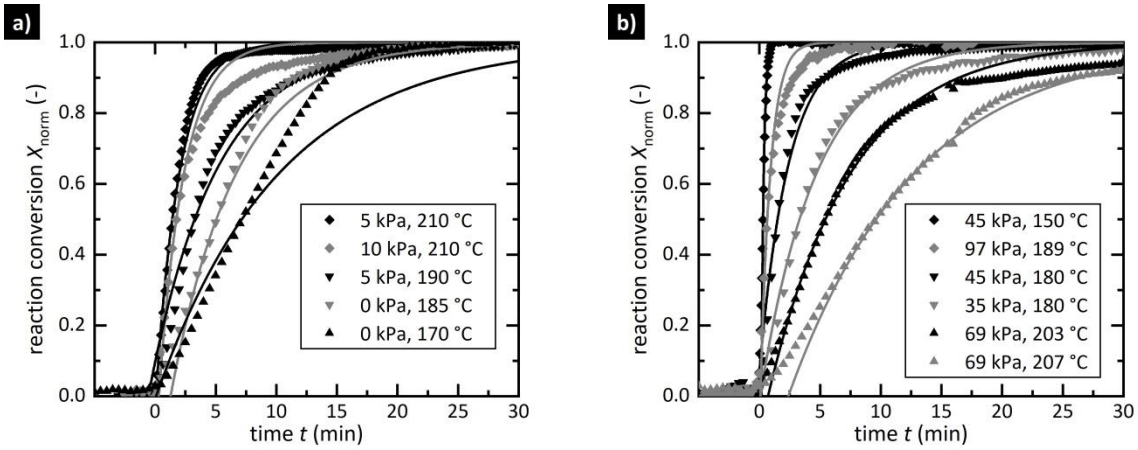

Fig. 10. Evaluation of the empirical rate models. The experimental data is given by the scatter plots; the corresponding results from the experimental rate models given in Eq. (17) and Eq. (19), respectively, are displayed as line plots in the same color. a) Dehydration reaction. b) Hydration reaction.

Similarly, in the case of the hydration reaction, the empirical model shows close agreement with experimental data for operation parameters which allow high reaction rates. For operation parameters closer to the equilibrium conditions, e.g. 69 kPa, 207 °C, the experimental reaction conversion shows a more sigmoidal progression, and hence, cannot be fully reproduced by the first-order rate model. To prove the validity range of the empirical model, the plot includes additional experimental data which are not considered in the determination of the rate model parameters (97 kPa, 189 °C). Still, even for this higher water vapor partial pressure, the empirical model predicts the reaction conversion with sufficient accuracy.

In general, in the range from approximately $0.1 < X_{norm} < 0.8$, the qualitative trend of the reaction conversion is accurately reproduced, so that the models parameterized in this work are considered valid empirical descriptions of the hydration and dehydration reaction rates of strontium bromide anhydrate.

3.4 Consequences for thermochemical storage applications

The performed material characterization study provides technically feasible charging and discharging temperatures as a function of the water vapor pressure. In a previous study, we have demonstrated the technical feasibility of distinct storage operation parameters, e.g. a minimum charging temperature of 179 °C (1 kPa condenser pressure) and a maximum discharging temperature of 281 °C (560 kPa evaporator pressure) [17]. With the *p,T*-correlations presented here, the operation parameters of the storage can be estimated for any other operation point within this range. E.g. for a given waste heat temperature of 120 °C (200 kPa) available for steam generation, the corresponding reaction temperature of the hydration reaction is 270 °C, according to Eq. (12. Assuming that a heat exchanger temperature gradient of 20 K is required to allow for a heat flux between the heat transfer fluid (HTF) and the storage, we conclude that the storage can be discharged at 250 °C HTF temperature. On the other hand, charging the storage e.g. at 210 °C HTF temperature (e.g. solar thermal energy or industrial waste heat) requires the condensation of the gaseous reactant at 7 kPa, see Eq. (11). Again, this estimation takes into account an internal gradient of 20 K in the heat exchanger. This vapor pressure corresponds to a condensation temperature of 40 °C, e.g. cooling with ambient air. The given operation points therefore result in an effective thermal upgrade by 40 K between the charging and the discharging temperature. Besides, the analysis of the effective reaction rates reveals 170 °C as the minimum temperature required for charging with technically relevant operation conditions: although charging the storage at lower temperatures is possible with moderate dehydration rates in water-free atmospheric conditions, this requires additional cooling effort to condense the water vapor emerging from the reactive material (e.g., below 15 °C).

Our results on the effective rates of reaction imply that the $SrBr_2/H_2O$ working pair is suitable for applications which require high specific thermal powers: e.g. for the discharging reaction running at 69 kPa and 200 °C, the effective rate coefficient $3.84 \cdot 10^{-3}$ 1/s implies that 80% of the storage's capacity can be discharged with specific thermal powers from 0.2 – 1.2 kW/kg $SrBr_2$, assuming a reaction enthalpy of 72 kJ/kg, the $SrBr_2$ molar weight 247 g/mol, and the first-order rate model described in Eq. (14). By choosing a higher steam pressure, these values can be further increased. Alternatively, for a lower discharge temperature and the same steam pressure (180 °C, 69 kPa), the specific power reaches values in the range of 0.9 – 4.4 kW/kg $SrBr_2$ (effective rate coefficients in Tab. 2). Correspondingly, running the charging reaction e.g. at 210 °C and 5 kPa results in specific thermal powers in the range of 0.5 – 2.5 kW/kg $SrBr_2 \cdot H_2O$ (effective rate coefficients in Tab. 1). However, the thermal power of an actual storage reactor is more likely determined by its design with regard to heat and mass transfer limitations. For instance, at distinct operating points (discharging at 208 °C, 150 kPa), the proof-of-concept storage reactor featured a maximum thermal power of 0.26 kW/kg $SrBr_2$ [17], and hence, was probably limited by heat transfer. Still, the empirical rate models developed and validated in this work are required to optimize the storage performance, e.g. by performing numerical studies on the packed bed heat exchanger design.

4 Conclusions

The hydration reaction of strontium bromide to its monohydrate phase and the dehydration reaction of the latter were identified as a promising thermochemical system for thermal energy storage and heat transformation. In this study, we report on the thermodynamic and kinetic properties and the cycle stability of the reactions. Our study includes examinations based on thermogravimetric analysis (TGA) as well as lab-scale experiments.

Pressure-temperature correlations describing the reaction temperatures for the dehydration and the hydration reactions are derived from the lab-scale setup in a pressure range from 1 kPa up to 150 kPa. The observed reaction temperatures stretch from approximately 160 °C up to 260 °C. At a steam pressure of 17 kPa, a thermal hysteresis of 14 K between the dehydration and the hydration reaction is observed. With the *p,T*-correlations presented here, the operation parameters of a $SrBr_2/H_2O$ thermochemical energy storage and heat transformers can be assessed in terms of charging/discharging pressures and temperatures.

To be able to assess the maximum thermal power allowed by the effective rate of reaction, we conducted kinetic studies in a temperature and pressure range relevant for typical storage applications. It is found that the rate of reaction slows down significantly when approaching thermodynamic equilibrium conditions not only in the case of the dehydration, but also in the case of the hydration reaction: here, at constant steam pressure, increasing temperatures effectively lead to lower reaction rates. For instance, when discharging at 180 °C and 69 kPa steam pressure, specific powers up to 4.4 kW/kg $SrBr_2$ were found in the TGA experiments. Furthermore, we developed empirical models for the hydration and the dehydration reactions which allow predicting the progression of the chemical reactions in a storage system operated under technically relevant operation conditions (hydration reaction: 30 – 97 kPa, 150 – 210 °C; dehydration reaction 0 – 10 kPa, 160 – 210 °C).

Cycle stability is experimentally proven in an isothermal TGA experiment for 100 hydration/dehydration cycles. Although the rate of the dehydration reaction decreases for conversions larger than 50% during cycling under low temperatures (170 °C), the reaction is fully reversible. Although no final statement can be drawn on the more long-term cycle stability or possible macroscopic changes when operated on larger scale, strontium bromide is a highly promising candidate for thermochemical energy storage and heat transformation.

5 Acknowledgements

The work described in this paper has received financial support from the “Bundesministerium für Wirtschaft und Energie” (BMWi, Federal Ministry for Economic Affairs and Energy) in Germany as part of the “TheSan” project (03ET1297A). We gratefully acknowledge the support of Marius Drexler and Stefan Wohnrau during the operation of the lab-scale setup and the TGA experimental campaign, respectively.

6 Nomenclature

Greek letters

ν	stoichiometric coefficient
ϑ	temperature, °C

Latin letters

A_0	pre-exponential factor, 1/s
$\Delta_R G$	Gibbs enthalpy of reaction, kJ/mol
$\Delta_R H^0$	standard molar enthalpy of reaction, kJ/mol
$\Delta_R S^0$	standard molar entropy of reaction, J/(mol·K)
E_a	activation energy, kJ/mol
$f(X)$	reaction model function
$h(p)$	pressure term
k	rate coefficient, 1/s
$k(T)$	Arrhenius term, 1/s
K_{fit}	reaction rate coefficient, 1/s
K_{eq}	equilibrium constant
m	mass, kg
n	pressure term exponent
p	pressure, kPa
p^0	reference pressure, kPa
R	universal gas constant, 8.314 J/(mol·K)
R^2	coefficient of determination
t	time, s
T	absolute temperature, K
X	reaction conversion

Indices

0	standard conditions for temperature and pressure (273.15 K, 1 atm)
dehyd	dehydration
eff	effective
exp	experimental
g	gas
hyd	hydration
norm	normalized
s	solid

Abbreviations

DSC	differential scanning calorimetry
HTF	heat transfer fluid
TG	thermogravimetric
TGA	thermogravimetric analysis

7 References

[1] Wongsuwan W, Kumar S, Neveu P, Meunier F. A review of chemical heat pump technology and applications. Applied Thermal Engineering. 2001;21:1489-519.
[2] Yu Y, Zhang P, Wu J, Wang R. Energy upgrading by solid–gas reaction heat transformer: A critical review. Renewable and Sustainable Energy Reviews. 2008;12:1302-24.
[3] Odukoya A, Naterer GF. Upgrading waste heat from a cement plant for thermochemical hydrogen production. International Journal of Hydrogen Energy. 2014;39:20898-906.
[4] Donkers PAJ, Sögütoglu LC, Huinink HP, Fischer HR, Adan OCG. A review of salt hydrates for seasonal heat storage in domestic applications. Applied Energy. 2017;199:45-68.
[5] Trausel F, De Jong AJ, Cuypers R. A review on the properties of salt hydrates for thermochemical storage. Energy Procedia. 2014;48:447-52.
[6] Richter M, Habermann E-M, Siebecke E, Linder M. A systematic screening of salt hydrates as materials for a thermochemical heat transformer. Thermochimica Acta. 2018;659:136-50.
[7] Afflerbach S, Trettin R. A systematic screening approach for new materials for thermochemical energy storage and conversion based on the Strunz mineral classification system. Thermochimica Acta. 2019;674:82-94.
[8] N'Tsoukpoe KE, Schmidt T, Rammelberg HU, Watts BA, Ruck WKL. A systematic multi-step screening of numerous salt hydrates for low temperature thermochemical energy storage. Applied Energy. 2014;124:1-16.
[9] Michel B, Mazet N, Neveu P. Experimental investigation of an innovative thermochemical process operating with a hydrate salt and moist air for thermal storage of solar energy: Global performance. Applied Energy. 2014;129:177-86.
[10] Michel B, Neveu P, Mazet N. Comparison of closed and open thermochemical processes, for long-term thermal energy storage applications. Energy. 2014;72:702-16.
[11] Esaki T, Kobayashi N. Reaction Rate Characteristics of SrBr2 Hydration System for Chemical Heat Pump Cooling Mode. Journal of Materials Science and Chemical Engineering. 2016;4:106-15.
[12] Cammarata A, Verda V, Sciacovelli A, Ding Y. Hybrid strontium bromide-natural graphite composites for low to medium temperature thermochemical energy storage: Formulation, fabrication and performance investigation. Energy Conversion and Management. 2018;166:233-40.
[13] Gilles D, Segato T, Courbon E, Degrez M, D'Ans P. Affordable Process for the Production of Strontium Bromide Used in Low Grade Heat Recovery Applications. Procedia CIRP. 2018;69:383-8.
[14] Glasser L. Thermodynamics of Inorganic Hydration and of Humidity Control, with an Extensive Database of Salt Hydrate Pairs. Journal of Chemical & Engineering Data. 2014;59:526-30.
[15] Wagman DD, Evans WH, Parker VB, Schumm RH, Halow I, Bailey SM, et al. The NBS Tables of Chemical Thermodynamic Properties. Selected Values for Inorganic and C1 and C2 Organic Substances in SI Units. Journal of Physical and Chemical Reference Data. 1982;11.
[16] Stengler J, Weiss J, Linder M. Analysis of a Lab-Scale Heat Transformation Demonstrator Based on a Gas–Solid Reaction. Energies. 2019;12:2234.
[17] Stengler J, Linder M. Thermal energy storage combined with a temperature boost: An underestimated feature of thermochemical systems. Applied Energy. 2020;262:114530.
[18] Perry DL. Handbook of Inorganic Compounds. 2011:581.
[19] Richter M, Bouché M, Linder M. Heat transformation based on CaCl2/H2O – Part A: Closed operation principle. Applied Thermal Engineering. 2016;102:615-21.

[20] Molenda M, Stengler J, Linder M, Wörner A. Reversible hydration behavior of CaCl2 at high H2O partial pressures for thermochemical energy storage. Thermochimica Acta. 2013;560:76-81.
[21] Sögütoglu L-C, Steiger M, Houben J, Biemans D, Fischer HR, Donkers P, et al. Understanding the Hydration Process of Salts: The Impact of a Nucleation Barrier. Crystal Growth & Design. 2019;19:2279-88.
[22] Wagner M. Thermal analysis in practice: fundamental aspects. 2018.
[23] Schmidt M, Linder M. Power generation based on the Ca(OH)2/ CaO thermochemical storage system – Experimental investigation of discharge operation modes in lab scale and corresponding conceptual process design. Applied Energy. 2017;203:594-607.
[24] Galwey AK, Brown ME. Thermal Decomposition of Ionic Solids: Chemical Properties and Reactivities of Ionic Crystalline Phases. 1999:596.
[25] Schaube F, Koch L, Wörner A, Müller-Steinhagen H. A thermodynamic and kinetic study of the de- and rehydration of Ca(OH)2 at high H2O partial pressures for thermo-chemical heat storage. Thermochimica Acta. 2012;538:9-20.
[26] Birkelbach F, Deutsch M, Werner A. The effect of the reaction equilibrium on the kinetics of gas-solid reactions — A non-parametric modeling study. Renewable Energy. 2020;152:300-7.